Supplementary information:

Revealing the active phase of copper during the electroreduction of CO_2 in aqueous electrolyte by correlating *in situ* X-ray spectroscopy and *in situ* electron microscopy

Juan-Jesus Velasco-Velez[1,2]*, Rik V. Mom[2], Luis-Ernesto Sandoval-Diaz[2], Lorenz J. Falling[2], Cheng-Hao Chuang[3], Dunfeng Gao[4,5], Travis E. Jones[2], Qingjun Zhu[1,2], Rosa Arrigo[6], Beatriz Roldan Cuenya[4], Axel Knop-Gericke[1,2], Thomas Lunkenbein[2], Robert Schlögl[1,2]

*Corresponding authors: velasco@fhi-berlin.mpg.de

[1]Department of Heterogeneous Reactions, Max Planck Institute for Chemical Energy Conversion, Mülheim an der Ruhr 45470, Germany.
[2]Department of Inorganic Chemistry, Fritz-Haber-Institut der Max-Planck-Gesellschaft, Berlin 14195, Germany.
[3]Department of Physics, Tamkang University, New Taipei City 25137, Taiwan.
[4]Department of Interface Science, Fritz-Haber-Institute of the Max-Planck Society, 14195 Berlin, Germany.
[5]State Key Laboratory of Catalysis, Dalian Institute of Chemical Physics, Chinese Academy of Sciences, 116023 Dalian, China
[6]School of Science, Engineering and Environment, University of Salford, 314 Cockcroft building, M5 4 WT, Manchester, U.K.

In situ Electrochemical flow cell with exchangeable working electrode

The main body of the electrochemical cell is made of polyether ether ketone (PEEK), which is electrically insulating and chemically inert. This cell has a Pt wire for a counter electrode and a Ag/AgCl reference electrode (FLEXREF, sourced from WPI Florida, USA). This setup was designed to use an exchangeable working electrode to allow the operation of different membranes with the same EC-cell as shown in Figure S9. The working electrode holder is compatible with the cell body used in the environmental scanning electron microscope (ESEM), FEI Quantan 200 FEG, allowing *in situ* electrochemical microscopy characterization (see Figure S10). For the *in situ* characterization of the electronic structure the EC flow cell is operated in the main chamber of the ISISS beamline in BESSY II (Berlin, Germany) which is equipped with a SPECS PHOIBOS 150 NAP hemispherical analyzer. The total fluorescence yield (TFY) signal is collected with an AXUV100 Opto Diode Corp which is located in the main chamber. Two different types of working electrode membranes were used during the experiments reported in this manuscript:

(a) Si_3N_4 based membrane: The pristine Si_3N_4 membranes (type NX10100C) were sourced from Norcada (Edmonton, Canada). This membrane is semi-transparent to the incoming X-ray and separates the electrolyte from the vacuum chamber were the photo-detector is located.

On the Si_3N_4 membrane (100 nm thick) a thin film of Cr (3 nm) adherence layer was deposited by physical vapor deposition (PVD). After that, 20 nm of Au were deposited onto the 3 nm Cr by PVD. We obtained a homogeneous polycrystalline thin film with a X-ray transmission through this membrane of approximately equal to 80% of the incoming intensity in the Cu $L_{2,3}$ edges range. The sealing of this cell is assured with a Kalrez O-ring of 0.7 cm diameter, yielding an effective working electrode area of ~0.4 cm^2 at a background pressure of ~10^{-7} mbar while the aqueous electrolyte circulates through the EC-cell. The continuous flow of electrolyte helps to eliminate the bubbles produced during the electrocatalytic reactions. The copper electrode was prepared by electrodeposition from 50 mM $CuSO_4$ at -0.7 V vs. Ag/AgCl during 60 s. The electrolyte was prepared by diluting 7.98 g of $CuSO_4$ (Sigma Aldrich, anhydrous powder, 99.99%) in 1 liter of Milli-Q water (18.2 MΩ) at room temperature (RT), 25°C and saturated with pure N_2 by gas bubbling through the electrolyte. This process yields the deposition of a copper electrode ~300 nm thick as shown in Figure S1A. After the electrodeposition of copper the cell was flushed with pure water and subsequently filled with 100 mM $KHCO_3$, which was prepared diluting 10 g of $KHCO_3$ (Roth, 99%) in 1 liter of Milli-Q water (18.2 MΩ) at room temperature and saturated with pure CO_2 by bubbling the electrolyte. To prove the operation of this cell, Video 1 shows the CA process at -1.8 V vs. Ag/AgCl where the bubbles formation is due to the CO_2RR and hydrogen evolution reaction.

(b) Graphene/ionomer membrane: This approach is based on a photoelectron semi-transparent membrane (a graphene layer transferred to an ionomer polymer) and allows the acquisition of spectra in the TEY/AEY/XPS modes. Chemical vapor deposited (CVD) graphene on a Cu film (18 µm thick with a roughness of 80 nm) and spin coated with Poly(methyl methacrylate) PMMA (model: 495 K, A2 and 60 nm thick) was sourced from the company Graphena (San Sebastian, Spain). The graphene layer is a continuous polycrystalline film with grain size in the range of ~20 µm, which was confirmed by scanning electron microscopy. The copper support was eliminated by floating on a 100 mM aqueous solution of $(NH_4)_2S_2O_8$ for 24 hours in order to assure that Cu is fully removed. The floating PMMA/graphene was transferred to another beaker filled with Milli-Q water in order to avoid the presence of $(NH_4)_2S_2O_8$ and copper dissolved in the electrolyte[1,2]. The 5 mm x 5 mm graphene/PMMA flake floating in Milli-Q water (DI-water) was transferred onto 1 cm wide disks of the FKD membrane sourced from Fumatek. The membrane was dried at room temperature for 24 hours. PMMA was removed by drops of acetone, which were, in turn, rinsed in water for one minute. Note that the acetone should be dropped only on the area coated with PMMA avoiding to wet the ionomer membrane which can be damaged by the acetone. The procedure was repeated five times to eliminate the PMMA. This process leaves a single layer of graphene of 5 mm x 5 mm on the FKD membrane, attracted by Van der Waals interaction. Using this electrode a continuous flow of 50 mM $CuSO_4$ (4.3 pH) was supplied to the cell, in order to accomplish the electrodeposition of copper on the graphene electrode at -1.6 V vs. Ag/AgCl during 120 s yielding an electrode of copper ~300 nm thick as shown in Figure S1B. After the electrodeposition of Cu onto the graphene electrode, the

$CuSO_4$ electrolyte was flushed out with pure water and replaced by 100 mM $KHCO_3$ (saturated in CO_2) aqueous electrolyte under continuous flow.

Potenstiostat

Potentiometric control was assured with a Biologic SP-300 device (Seyssinet-Pariset, France), allowing for different potentiometric and amperometric controls.

CO_2 electroreduction measurements

CO_2 electroreduction measurements were carried out in a gas-tight H-cell separated by an anion exchange membrane (Selemion AMV, AGC Inc.). Both, working electrode and counter electrode compartments were filled with 40 mL 0.1 M $KHCO_3$ (Honeywell Fluka, 99.7%) and purged continuously with CO_2 (99.995%, 20 mL min^{-1}). A $KHCO_3$ solution was prepared with ultrapure water and further pre-purified with Chelex 100 Resin (Bio-Rad, 100−200 mesh)[3]. Prior to the measurement, the electrolyte was bubbled with CO_2 for 30 min to remove oxygen in the solution and saturate the solution. The electrolyte was continuously mixed using a magnetic stirrer. A platinum gauze (MaTecK, 3600 mesh cm^{-2}) was used as the counter electrode and a leak-free Ag/AgCl/3.4 M KCl electrode (Innovative Instruments, Inc.) as reference electrode. The sample (Cu electrodeposited on Au mesh) was used as working electrode and was contacted with a clamp wrapped by Kapton tape to avoid unwanted reactions. The potentials were controlled with an Autolab potentiostat (PGSTAT 302N). The gas products were analyzed by online gas chromatography (GC, Agilent 7890A) every 17 min. CO, H_2, and hydrocarbons were separated by different columns (Molecular sieve 13X, HayeSep Q, and Carboxen-1010 PLOT) and quantified by a thermal conductivity detector (TCD) and flame ionization detector (FID).

Calculation of the Faradaic efficiency of gas products:

$$\mathrm{f}_{gas} = \frac{f_{flow} \times c_{gas} / V_m \times n \times F}{I \times 60} \times 100$$

f_{gas}: Faradaic efficiency of gas product, %;

f_{flow}: flow rate of CO_2, mL min^{-1};

I: electrolysis current, A;

c_{gas}: volume ratio of gas product, determined by online GC;

V_m: the molar volume of an ideal gas at 1 atmosphere of pressure, 22400 mL mol^{-1};

n: number of transferred electrons for certain product;

F: Faraday´s constant, 96485 C mol^{-1}.

Process reversibility investigation

The reversibility of the process was investigated comparing the spectra obtained with the bulk (XAS-TFY) and surface (XAS-TEY) sensitive techniques, full set of collected spectra and electrochemical performance are shown in Figures S7 and S8. Figure S11A shows the comparison of the spectra at OCV, during CO_2RR and OCV after reaction in a XAS-TFY fashion (bottom graphics represent the spectra difference). According to the experiments reported here, the electrode is reduced under CO_2RR from a copper mixed oxide (40% Cu^0 and 60% Cu^+) to metallic copper. On the other hand, the surface sensitive spectra (Figure S11B) also reveals a reduction of a mixed copper oxide (with a composition of 25% Cu^0, 45% Cu^+ and 30% Cu^{2+}) to metallic copper indicating that the oxidation state for copper is exactly the same in the surface and bulk following the Pourbaix diagram[4] (see Figure S5). Thus, the two peaks ascribed to Cu^+ and Cu^{2+} are suppressed during the CO_2RR as the difference of the spectra between OCV and during CO_2RR show (black line at the bottom of Figure S4S11A). Meanwhile, the bulk, which initially is mostly composed of Cu^+ species, is also reduced during the CO_2RR. On the other hand, the surface sensitive measurements show that when the potential is back to OCV the electrode undergoes re-oxidation with a pronounced feature of Cu^{2+} appearing and with minor contribution of Cu^+ species also apparent. Note that the re-oxidation of the surface takes place immediately after the CO_2RR potential is removed but the re-oxidation of the bulk has slower kinetics. In other words, the OCV potential changes depending on time after the CO_2RR potential is suppressed, as shown in Figure S12 collected in TFY. This result clearly indicates that the *ex situ* characterizations of the electrode cannot address the nature of the catalytic sites during reaction as far as the oxidation state change with time once the reaction process is stopped. Furthermore, Figure S12 stresses the importance of *in situ* and *operando* studies. These measurements prove that the reduction/oxidation kinetics are fast allowing the electrode to get close equilibrium before and after CO_2RR, where the Cu^{2+} species dominate the surface and Cu^+ the bulk under OCV conditions. Finally, we should indicated that the spectra reversibility exclude the possibility that the X-ray beam is responsible for the reduction of the electrode.

Electron-beam interaction with the sample

The interaction of the electron-beam with the electrode in the electrochemical cell based on the Si_3N_4 membrane was investigated. It was found that electrochemical performance is not affected by the electron-beam but the observed processes can be accelerated. This effect is clearly visible in videos 2 and 3. Thus, it is possible to deposit and dissolve the copper reversibly depending on the applied potential as shown in video 2. However, as it is shown in video 3 (lower magnification) the part that was previously exposed to the electron beam (high

magnification) can be deposited and dissolved with copper much faster than the area not illuminated previously by the beam. We ascribe this effect to the fact that the e-beam probably cleans the gold electrode surface due to the formation of radicals by water radiolysis that react with remaining coating contamination. Higher magnification can yield the formation of micro gas bubbles from the radiolysis process as a consequence of high density of electrons per area. It is noteworthy that this techniques enables the true monitoring of corrosion processes as the dissolution of copper prompted by the application of anodic polarization which is shown in video 4.

The effect of the electron-beam in the polymer cation exchange membrane (CEM) was investigated under different conditions. Video 5 shows the effect of the beam in a pristine membrane coated with graphene, thus no apparently effects are observed at this magnification. However, under higher magnification the membrane is highly sensitive to the beam (Figure S13A). The beam effect hinders the ions transport through the membrane as indicate the presence of square shape with no deposited copper observed for example in Figure S13B. However, in presence of electrodeposited copper thin film, this effect is suppressed. We guess that this electron-beam interaction with matter is enhanced in pristine CEM due to its lack of electrical conductivity, however the addition of a conductive thin film mitigates drastically this interaction. Furthermore, we found beam induced radiolysis process at high magnifications in the confined electrolyte in areas with low electrical conductivity and highly hydration as proves by the bubbles formation in video 6. To mitigate the electron-beam matter interaction we reduced the beam dose, we performed electron-beam on and off measurements and also we investigated the electrode in areas not exposed to the electron beam. By doing so, we avoided/mitigated this interaction.

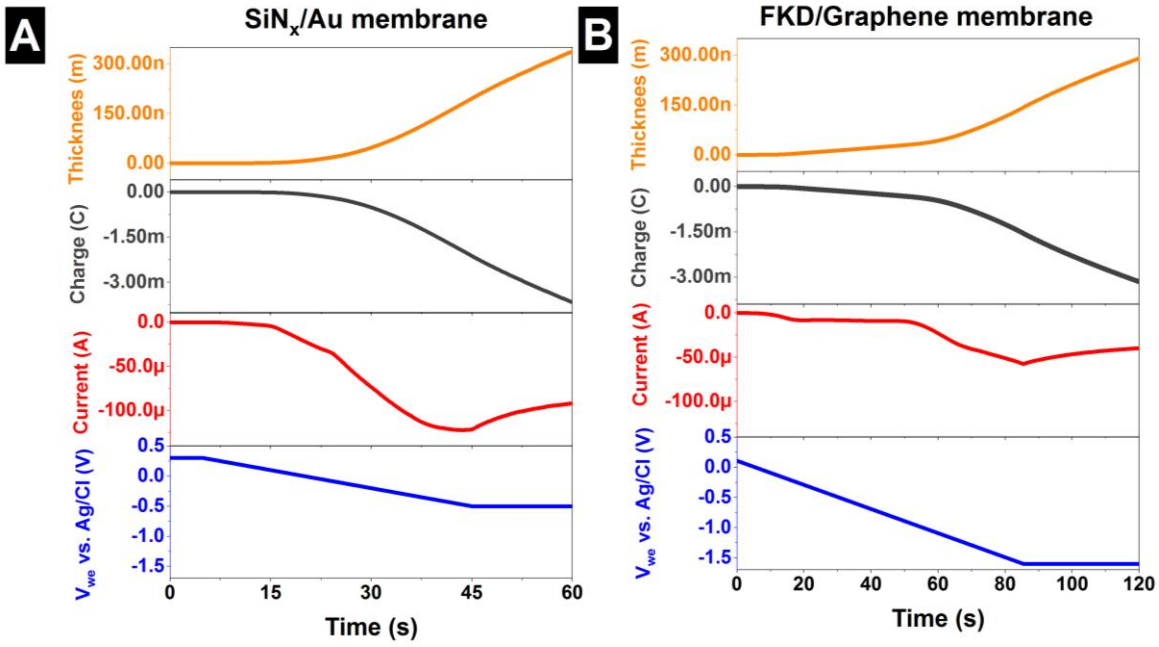

Figure S1: Estimated thickness (d) from the total charge transferred: $d = (M_{Cu} \cdot Q_T)/(\rho_{Cu} \cdot A \cdot n_{Cu} \cdot F)$, where M_{Cu} is the molar mass of copper, Q_T is the total charge transferred, ρ_{Cu} is the density of copper, A is the electrode effective area, n_{Cu} is the valence of copper and F the Faraday's constant. **A** Si_3N_4 and **B** FKD/Graphene membranes.

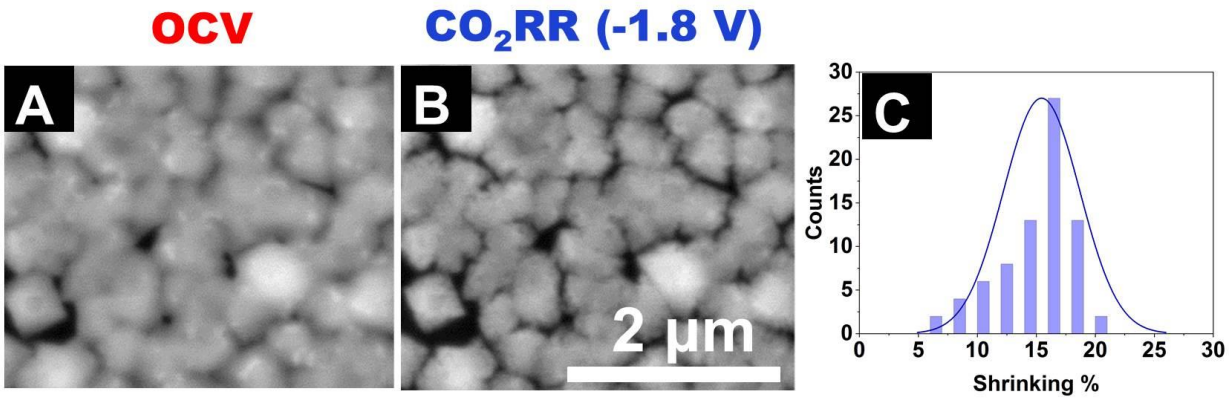

Figure S2: *In situ* SEM measurements in 100 mM $KHCO_3$ saturated in CO_2 under **A** OCV and **B** CO_2RR conditions with the Si_3N_4 membrane electrochemical cell. **C** Relative shrinking distribution.

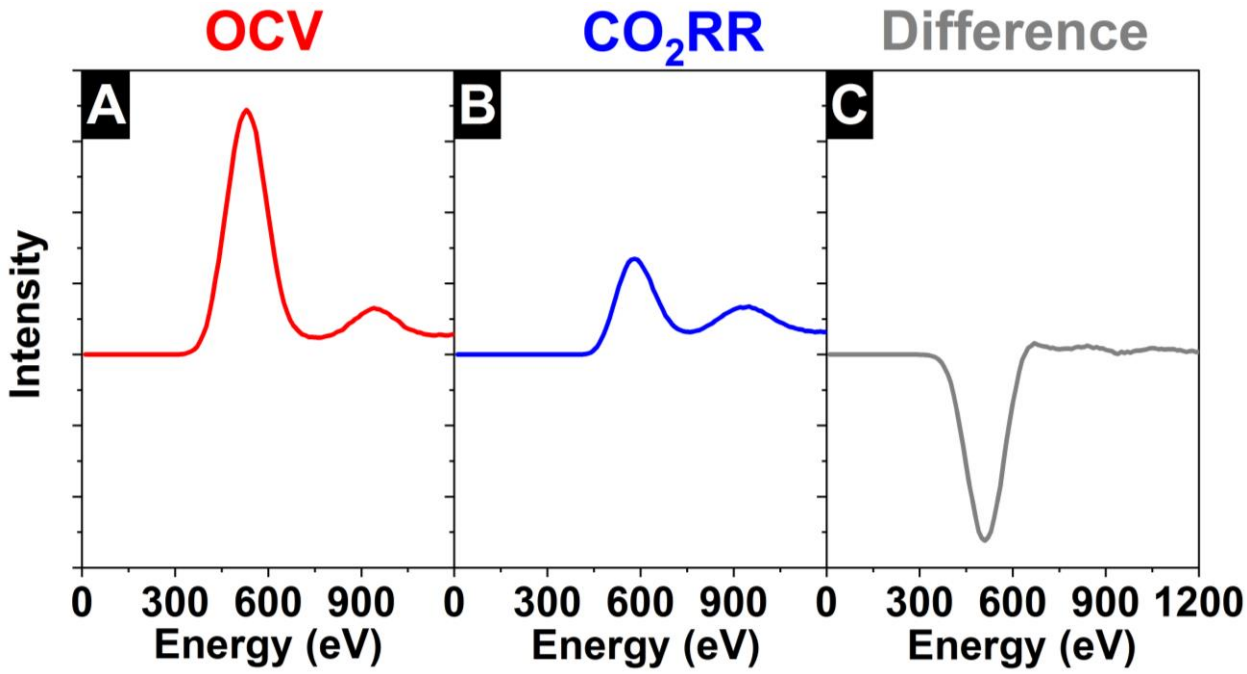

Figure S3: *In situ* EDX collected with the Si_3N_4 membrane (100 nm thick) and electrodeposited Cu electrode onto a 20 nm thick PVD gold electrode under **A** OCV and **B** CO_2RR conditions. **C** Difference.

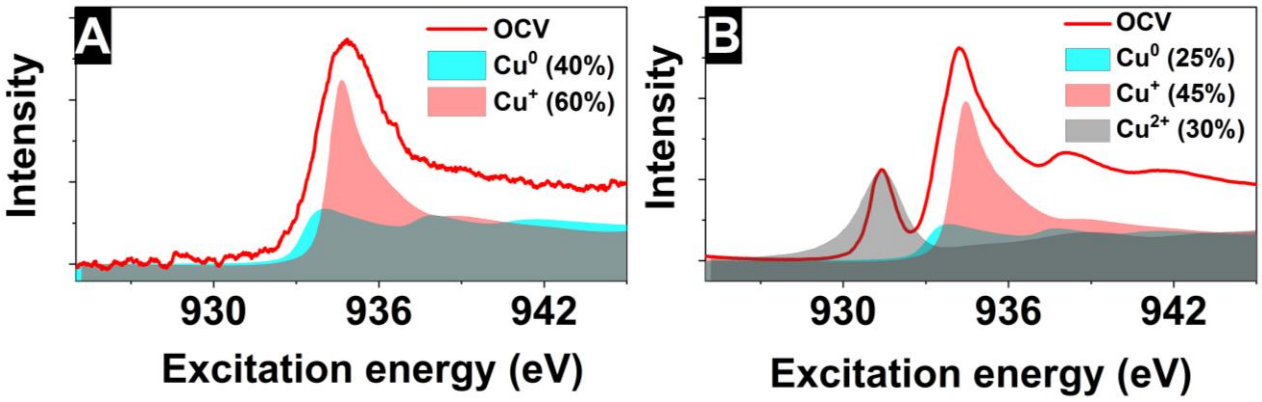

Figure S4: XAS Cu L_3 absorption edge measured **A** with the Si_3N_4 cell (TFY) and **B** with the Graphene/FKD cell (TEY) as well as the linear combination of relevant copper reference samples that resembles the spectra collected.

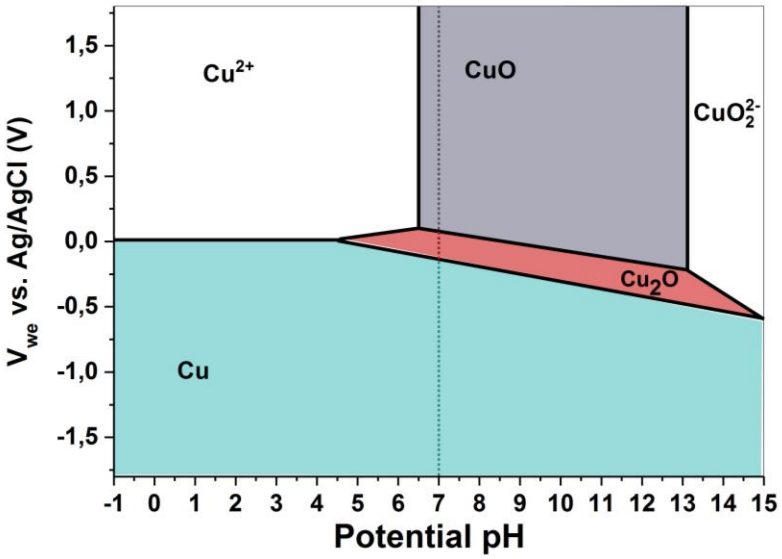

Figure S5: Pourbaix diagram for copper[4].

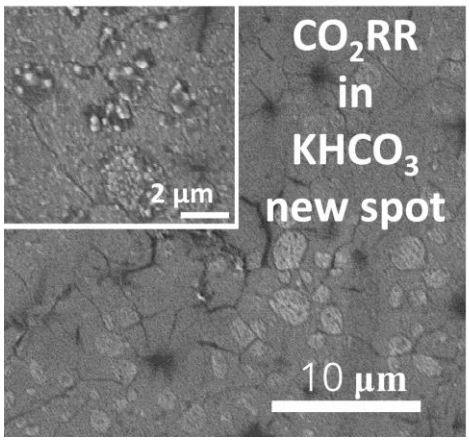

Figure S6: *In situ* SEM measurements in 100 mM $KHCO_3$ saturated in CO_2 under CO_2RR with the graphene/ionomer membrane.

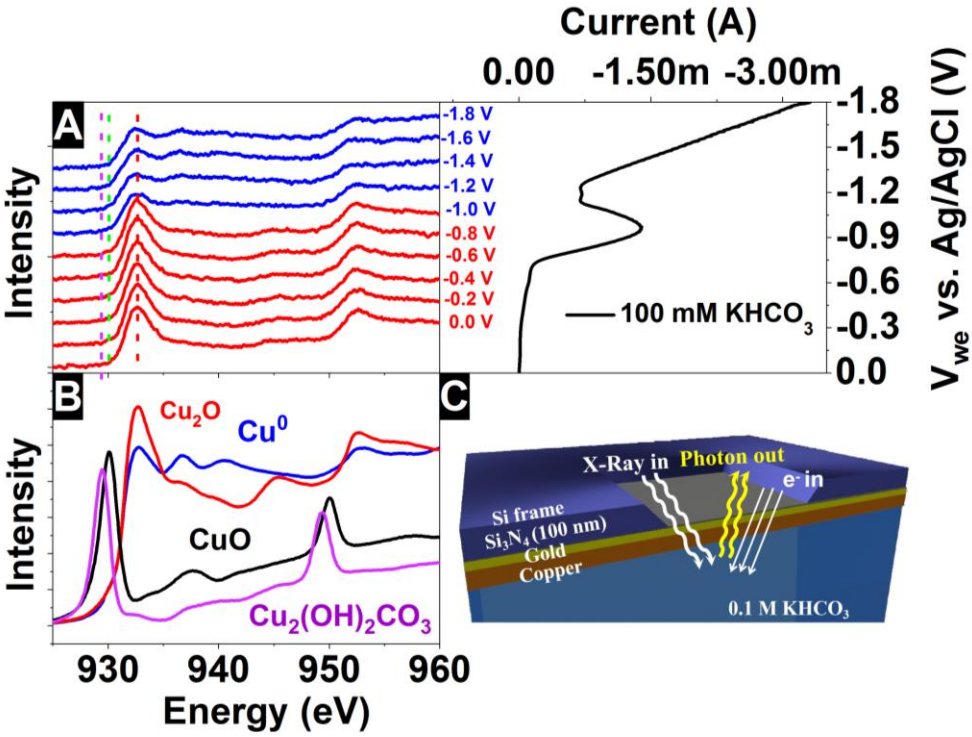

Figure S7: A XAS measurements in TFY and corresponding LSV in 100 mM $KHCO_3$. **B** References Cu $L_{2,3}$-edge spectra of different samples. **C** Schematic drawing of the approach used to investigate electrified electrodes (surface and bulk), which is composed of: a semi-transparent Si_3N_4 membrane (100 nm thick) and electrodeposited Cu electrode onto a 20 nm thick gold electrode.

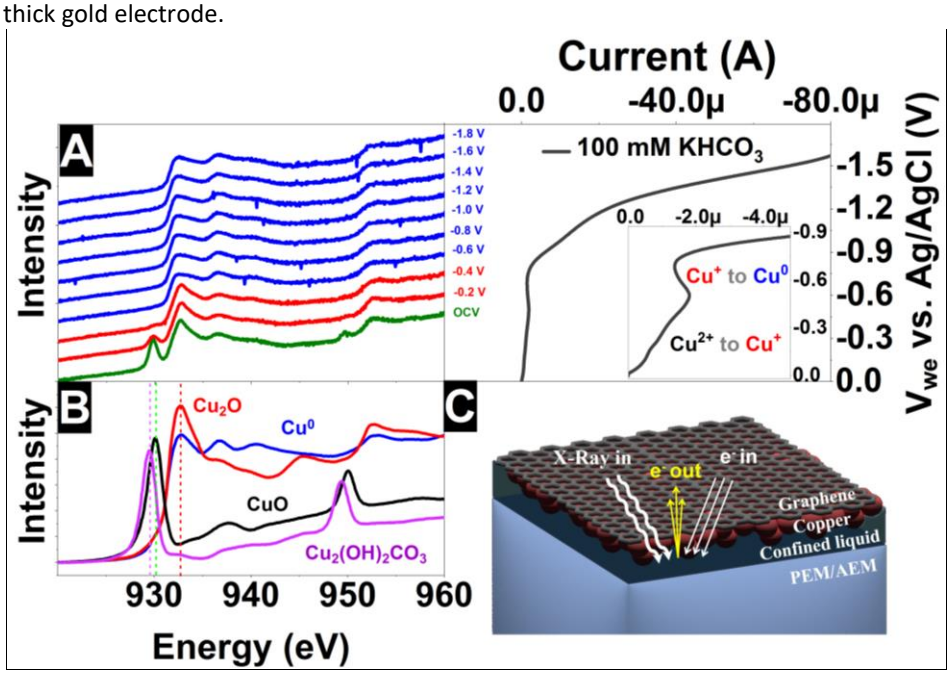

Figure S8: A XAS Cu $L_{2,3}$ edges spectra collected in TEY and corresponding LSV related to the CO_2RR (inset: LSV of the reduction waves). **B** References copper samples. **C** Schematic drawing of the approach used to investigate electrified interfaces, which is composed of: a semi-transparent graphene membrane for the photoelectrons as well as electrode, electrodeposited copper, confined electrolyte and a cation exchange membrane (CEM).

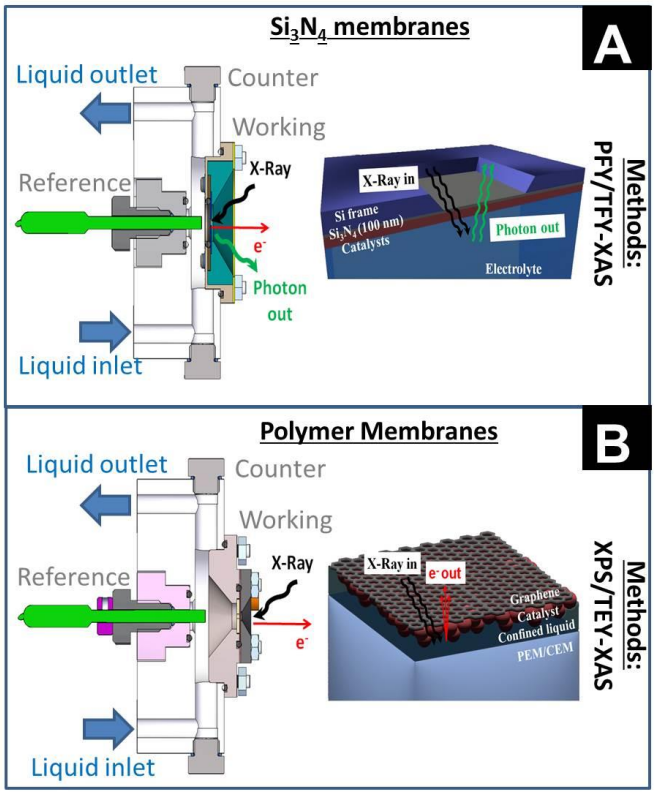

Figure S9: Drawings of the EC-cell used for the experiments including to type of exchangeable electrodes: **A** Si_3N_4 and **B** graphene/ionomer (bottom) membranes.

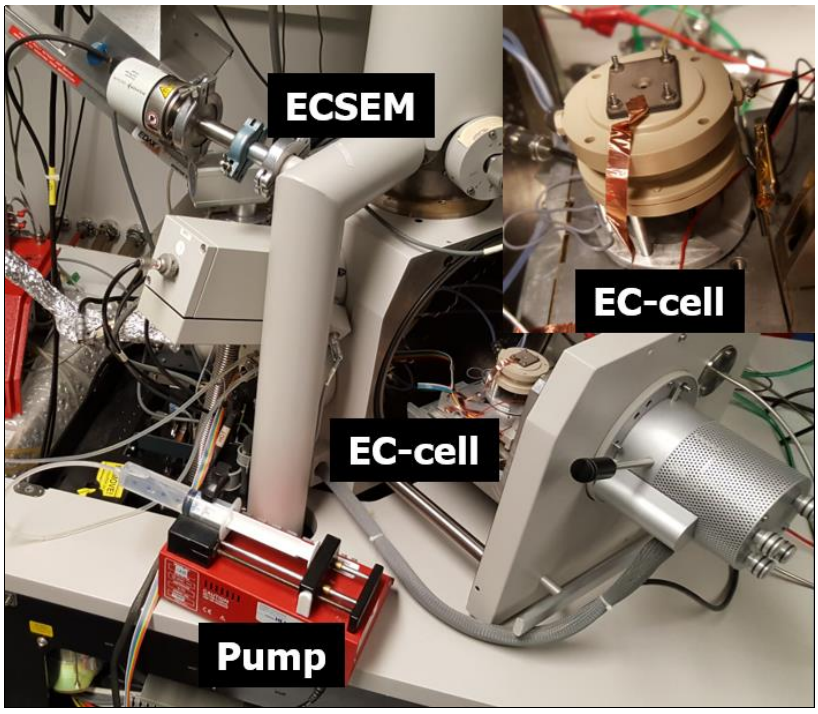

Figure S10: Picture of the ECSEM and electrochemical cell.

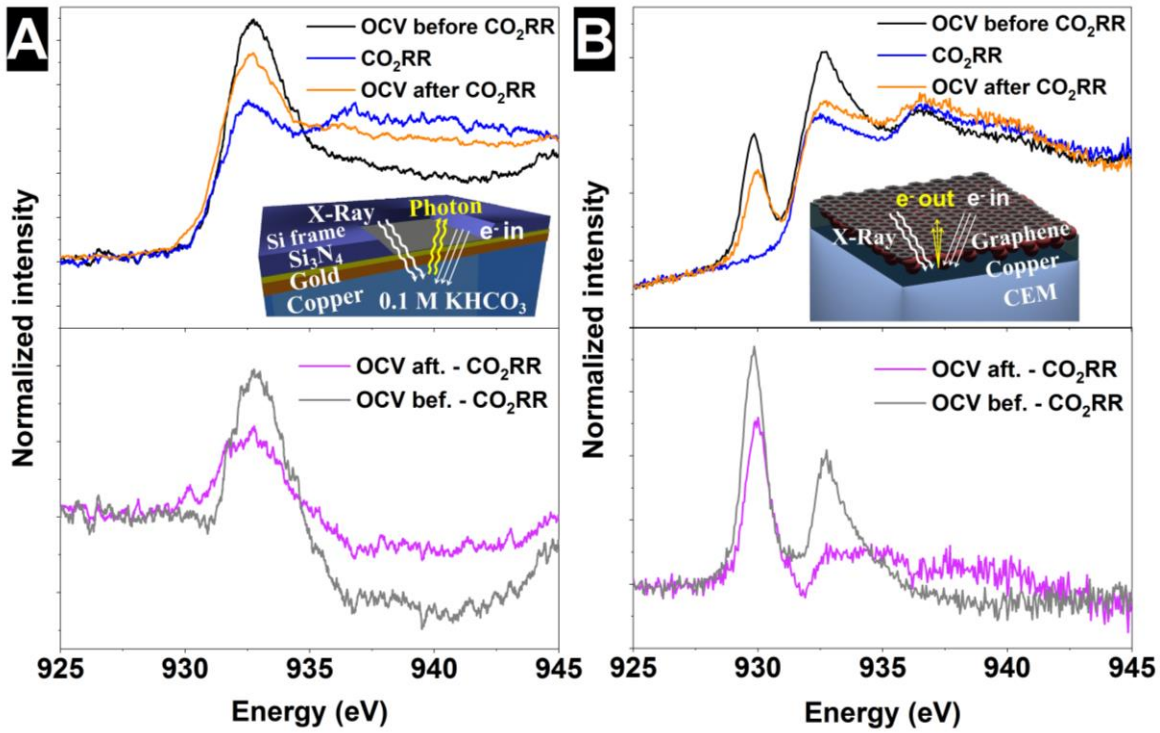

Figure S11: XAS Cu L_3-edge spectra collected under OCV and CO2RR conditions (top) and spectra difference (bottom): **A** with the Si_3N_4 (TFY) and **B** graphene/ionomer (TEY) membrane setups.

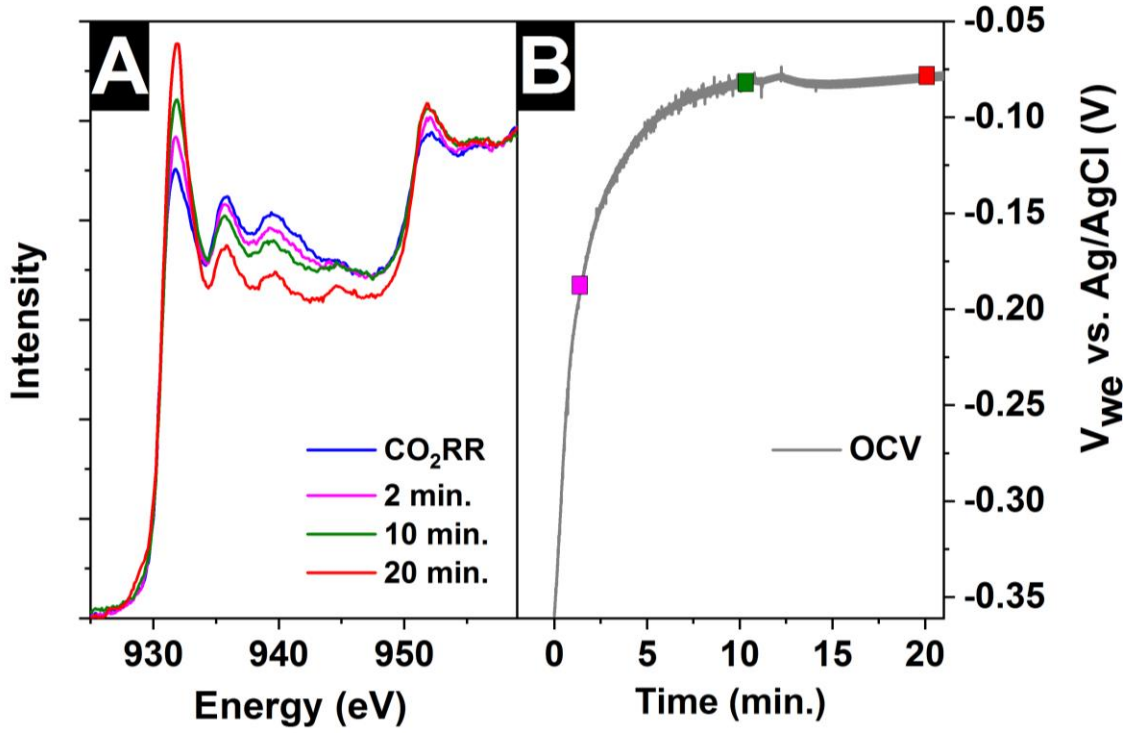

Figure S12: A TFY-XAS Cu $L_{2,3}$ edges spectra depending on time after the CO_2RR and the variation of the **B** OCV depending on time.

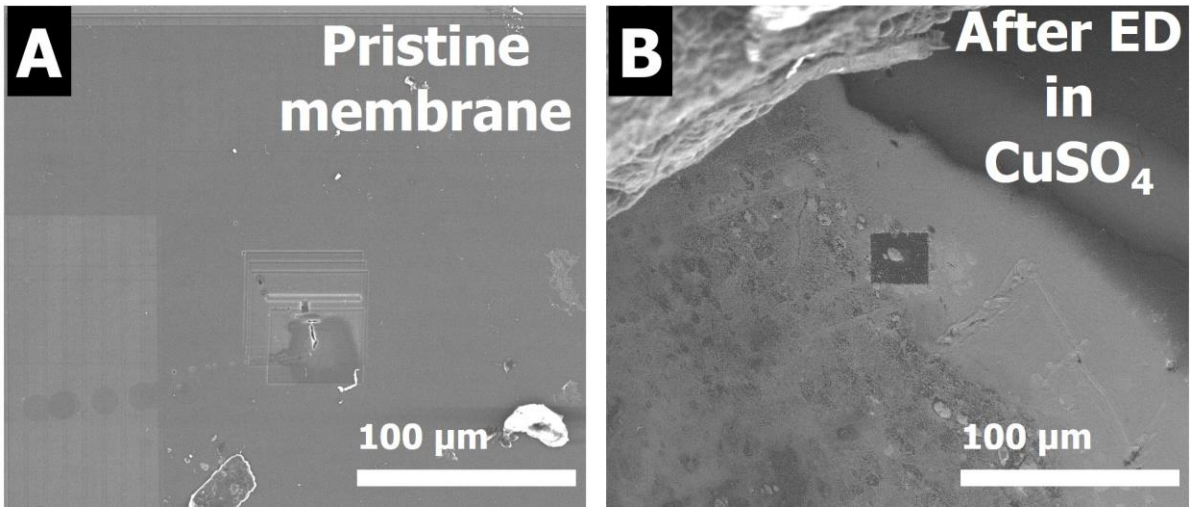

Figure S13: A Beam damage induced in the pristine membrane. **B** Ions transport hinders in the area affected by beam damage.

References:

(1) Velasco-Vélez, J. J.; Pfeifer, V.; Hävecker, M.; Wang, R.; Centeno, A.; Zurutuza, A.; Algara-Siller, G.; Stotz, E.; Skorupska, K.; Teschner, D.; Kube, P.; Braeuninger-Weimer, P.; Hofmann, S.; Schlögl, R.; Knop-Gericke, A.; Atmospheric pressure X-ray photoelectron spectroscopy apparatus: Bridging the pressure gap. *Rev. of Sci. Ins.* **2017**, 87, 053121.

(2) Velasco-Vélez, J. J.; Teschner, D.; Girgsdies, F.; Hävecker, M.; Streibel, V.; Willinger, M. G.; Centeno, A.; Willinger, M. G.; Cao, J.; Lamoth, M.; Frei, E.; Wang, R.; Centeno, A.; Zurutuza, A.; Hofmann, S.; Schlögl, R.; Knop-Gericke, A.; The role of adsorbed and subsurface carbon species for the selective alkyne hydrogenation over a Pd-black catalyst: an operando study of bulk and surface. *Topics in catalysis* **2018**, 61, 2052-2061.

(3) Gao, D.; Scholten, F.; Roldan Cuenya, B. Improved CO_2 electroreduction performance on plasma-activated Cu catalysts via electrolyte design: halide effect. *ACS Catalysis* **2017**, 7, 5112-5120.

(4) Pourbaix, M., Atlas of electrochemical equilibria in aqueous solutions. 2d English ed. **1974**, Houston, Tex.: National Association of Corrosion Engineers.